Received: 24 February 2022 | Revised: 4 July 2022 | Accepted: 18 July 2022

DOI: 10.1002/htj.22655

ORIGINAL ARTICLE

HEAT TRANSFER WILEY

Insight into the heat transfer across the dynamics of Carreau fluid subject to inclined Lorentz force conveying tiny particles and motile gyrotactic microorganisms: The case of stratification

E. O. Fatunmbi[1] | **I. L. Animasaun**[2,3,5] | **A. S. Oke**[4] | **S. O. Salawu**[5]

[1]Department of Mathematics and Statistics, Federal Polytechnic, Ilaro, Nigeria

[2]Department of Mathematical Sciences, Fluid Dynamics and Survey Research Group, Federal University of Technology Akure, Akure, Nigeria

[3]Department of Mathematical Sciences, United Arab Emirates University, Al Ain, Abu Dhabi, United Arab Emirates

[4]Department of Mathematics, Landmark University, Omu-Aran, Nigeria

[5]Department of Mathematics and Actuarial Science, Kenyatta University, Nairobi, Kenya

Correspondence
I. L. Animasaun, Department of Mathematical Sciences, Fluid Dynamics and Survey Research Group, Federal University of Technology Akure, Akure PMB 704, Nigeria.
Email: anizakph2007@gmail.com

Abstract

Sequel to the usefulness of exploration of Carreau fluid flow for understanding the nature of the shear thinning and thickening characteristics of industrial fluids and polymer suspensions, nothing is known on the heat transfer across the dynamics of Carreau fluid subject to three kinds of stratification (i.e., thermal, concentration, and diffusion of motile microorganisms). In this article, the motion mentioned above when inclined Lorentz force, haphazard motion of tiny particles, thermophoresis, and motile gyrotactic microorganisms are significant is presented, explored, and deliberated upon. Similarity transformation variables were employed to reduce the model from partial to ordinary differential equations. The Runge–Kutta–Gill methodology was used in conjunction with the shooting method and MATLAB bvp4c to obtain the numerical solution. It is worth concluding that thermal stratification and wall heating/temperature ratio terms promote heat transmission while increasing the size of the Weissenberg number and the mixed convection parameter lowers the skin friction coefficient. Furthermore, it has been shown that when stresses grow,

viscosity promotes the deformation of fluid components, resulting in fluid velocity retardation.

KEYWORDS
Brownian motion, Carreau nanoliquid, motile microorganism, nonlinear radiation, temperature-dependent properties

1 | INTRODUCTION

Exploration of Carreau fluid flow is useful for understanding the nature of the shear thinning and thickening characteristics of industrial fluids and polymer suspensions in various flow modes. Some of the classifications of fluids are non-Newtonian fluid with either time-dependent viscosity or time-independent viscosity, viscoelastic fluid, and Newtonian fluid; Animasaun et al.[1] However, certain categories of fluids exhibit relaxation time as they flow due to changes in the shear rate, viscosity at an infinite shear rate and viscosity at zero shear rate. According to Shamshuddin et al.,[2] Carreau fluid is an important phenomenon for oil purification research, with an emphasis on the dynamics of Carreau fluids over a stretchable surface experiencing magnetic field interaction. According to Ahmad et al.,[3] dynamics of Carreau fluid suit Newtonian fluid and power-law fluid flows due to the fact that the viscosity varies with not only the shear rate but also temperature change; see Jangili et al.[4] and Hassan et al.[5] In a study on hydromagnetic with temperature-dependent viscosity on axisymmetric surfaces, Barakat[6] discovered that when the temperature distribution grew, the quality of the fluid viscosity reduced with time. The outcome of another study on the electromagnetic fluid in stretchy media by Mahmoud,[7] the material viscosity was found to steadily reduce as heat propagation increased. Salawu et al.[8] demonstrated the irreversibility and criticality of magneto-couple stress material under Navier slip settings with varying fluid characteristics. It was discovered that for effective fluid utilization, energy loss may be avoided by rising thermodynamic equilibrium. Pratumwal et al.[9] used a U-tube viscometer to investigate the effects of the Carreau–Yasuda and power-law models on blood viscosity. Temperature differences, as shown in image scanning, have a considerable impact on blood viscosity. The transient flow of heat transfer magneto-Carreau fluid via a stenosis artery was studied by Abdollahzadeh Jamalabadi et al.[10] The Carreau flow was shown to be pulled through the arterial media by the magnetic field. As a result, the impact of varied heat-dependent characteristics on hydromagnetic fluid shear viscosity cannot be overstated.

The inclusion of motile microorganisms in a magneto-Carreau moving liquid expands its application possibilities in fields (i.e., technology, engineering ecology, and biomedical technology). Denser microorganisms, such as gyrotaxis, oxytaxis, algae, and bacteria, produce suspension patterns at the upper surface of a fluid, resulting in biconvective flow, according to Vadasz.[11] The bioconvection flow is induced by stratified unsteady density and reactant species transfer, both of which are required in biomicrosystems; see Tsai et al.[12] and Yusuf et al.[13] According to Nima et al.,[14] a bioconvection flow mechanism can create hydromagnetic system instability and can be constantly adjusted for propulsion and aggregate microorganism architectures. As a result, Kuznetsov and Avramenko[15]

examined biconvection of tiny particle stability for gyrotactic suspension microorganisms in a finite depth layer. The tiny density particles are proven to be elevated by increasing the Rayleigh number, indicating that stable suspension is seen with particle support. Non-Newtonian biconvective microorganism fluid flow in a porous tube was studied by Beg et al.[16] It was observed that up-swimming of motile bacteria assisted fluid heat transfer. Mahdy[17] looked at the natural convection flow of gyrotactic microorganism nanofluid across a saturated porous boundary layer cone. The motile gyrotactic microorganism interaction accelerated nanoparticle heat conduction and thermal conductivity, as previously observed. Han et al.[18] have used a digital biosensor to study marine pollution of a moving microalgal diluter-based microfluidic. The temperature field was said to be influenced by the sensitivity and density of the strain's algal cell. Of recent, Song et al.[19] assessed the impact of thermal Sutterby fluid composed of tiny particles in the presence of gyrotactic microorganisms, variable thermal and concentration conductivity with solutal and Marangoni boundaries over an elongated cylinder. The numerical report indicated that thermal conductivity and surface convection terms boost the nanofluid heat distribution.

For decades, the need to increase industrial productivity has renewed interest in overcoming the barrier of poor heat convection and heat conduction of fluid materials. Choi[20] examined the addition of nanometer-sized carbides, oxides, and metal to a base fluid (e.g., ethylene glycol, oil, and water) to increase fluid heat convection and conduction, and concluded that fluid heat transfer is improved. This discovery sparked scientists' and researchers' interest in nanofluids as a means of increasing the heat transfer mechanism of various devices. Qayyum et al.[21] pointed out the usefulness of nanofluids in the cooling of high heat flux machines in welding equipment (e.g., high power laser diode arrays and microwave tubes), electronic devices, such as microprocessors, transportation as well as energy generation. Nanofluids have unique features that make them suitable for use in a variety of heat transfer systems, including microelectronics, solar collectors, cancer therapy, fuel cells, household refrigerators, pharmaceutical operations, engine cooling thermal management, hybrid-powered engines, boiler flue gas temperature reduction and heat exchanger, and many more; see Salawu et al.,[22] Fatunmbi and Salawu,[23] and Khan et al.[24] Hayat et al.[25] investigated the motion of electrically conducting second-grade nanofluid induced by stretching sheet using the Buongiorno model characterized by Brownian motion and thermophoresis effects. Ijaz Khan and Alzahrani[26] performed a numerical simulation for the micropolar nonlinear mixed convective transport via the Buongiorno model with the impact of chemical reaction. It is worth deducing from the reports of Kuznetsov and Avramenko,[15] Beg et al.,[16] and Mahdy[17] that the suspension of bioconvective gyrotactic microorganism phenomena in a nanofluid is a promising platform for increasing heat convection and conduction of nanoparticles in the base liquid. Nanofluid flow slip and heat transmission over an endless stretching plate were examined by Niu et al.[27] The numerical results revealed that bioconvection has a significant impact on the mass transfer and heat conductivity of the microbe nanoparticle. Fatunmbi and Adeosun[28] investigated the features of heat and mass transport in the motion of reactive Eyring–Powell nanoliquid across a vertical Riga device caused by exponential fluctuation of dynamic fluid viscosity, convective wall condition, thermal radiation, and viscous dissipation. Despite the combined impact of magneto-Carreau flowing fluid and the gyrotactic moving microbe in producing bioconvection for improving nanoparticle thermal convection and conduction, only a small amount of research has been done. Oke et al.[29]

investigated the effect of volume fraction and heat source/sink on the motion of water transporting 47 nm alumina nanomaterials along a uniform surface, whereas Kinyanjui Kigio et al.[30] used a numerical technique to investigate hydromagnetic Casson nanofluid flow in a vertical sheet, which included volume fraction analysis and convective heat transfer. Stagnation-point flow in tangent hyperbolic nanoliquids with thermophoresis and Brownian movement coupling activation energy was studied by Fatunmbi et al.[31] The intensity of heat and mass transmission was found to have reduced due to an increase in the magnitude of microscopic particle thermomigration. Song et al.[32] adopted the Buongiorno model to publicize the impact of haphazard movement and thermal migration of two different water and ethylene glycol-based nanoparticles over a convectively heated surface. Lately, Mabood et al.[33] communicated the transport of hydromagnetic Jeffrey fluid conveying nanoparticles along a stretching surface comprising a wide range of engineering application physical terms. Other related published facts on the dynamics of related fluids had been presented by Khan et al.[34–37]

Stratification in fluids is caused by differences in temperature and concentration, as well as density fluctuations. This phenomenon indicates a production or deposition of layers in a vertical orientation which is usually seen in many natural, engineering as well as in industrial activities and environments. Thermal stratification in reservoirs and oceans, energy storage systems such as solar ponds, and heat transport from thermal sources, such as groundwater reservoirs and oceans, power plant condensers, heterogeneous mixtures in the atmosphere and groundwater reservoirs, salinity stratification in rivers, and heat discharge into the atmosphere are all common examples of such phenomena; Koriko et al.,[38] Rehman et al.[39] Due to these uses, Atif et al.[40] investigated the motion of an electroconducting double stratification micropolar nanofluid consisting of a motile gyrotactic creature with Joulean heating, radiative heat, thermophoresis, and Brownian motion. Due to the substantial stratification effect and fluid material term, the numerical simulation indicated a damping temperature profile. Later, Ijaz and Ayub[41] employed a homotopy analysis approach to describe reactive Walter-B nanoliquid transport across a stretched material plate with double stratification accompanying unequal heat source and activation energy. The analytic solution revealed that when temperature and concentration stratification increase, the thermal and solute fields decrease. In the presence of a thermal heat source, Sarojamma et al.[42] explored the problem of dual stratification coupling nonlinear radiative heat distribution in magneto-micropolar fluid motion induced by an extended sheet. The stratification parameter caused a slowing velocity, according to the researchers. The goal of this study is to investigate magneto-Carreau nanofluid flow using gyrotactic motile microorganisms and different material characteristics. This is prompted by the suggestion of Nima et al.[14] for future expansion, as well as the findings by Abbas et al.[43] and Shah et al.[44] This investigation is relevant in hydromagnetic lubricant, ecological engineering, microsystems, and others in boosting industrial productivity and biotechnology. As a result, different flow characteristics are investigated in response to changes in thermal reaction fluid parameters. For a thorough understanding of the fluid parameters' influence, a numerical analysis of the dimensionless model is performed, with the results displayed in tables and graphs. Specifically, the present study has been investigated to provide answers to the following questions:

1. What significant impact does a rise in the exponential space-based heat source, wall heating/temperature ratio term, viscosity, thermophoresis, and thermal radiation parameters have on the mechanism of temperature distribution of Carreau fluid conveying tiny particles?

2. What effect do the emerging physical parameters have on the velocity, temperature, concentration, and motile microorganism profiles?
3. How does the skin friction coefficient of the Carreau fluid conveying tiny particles react with a higher magnitude of viscosity parameter, Weissenberg number, inclination angle of the magnetic field, mixed convection parameter, and magnetic field parameter?
4. What significant changes occur in the dynamics of heat transfer when Carreau nanofluid thermal stratification, wall heating/temperature ratio parameter, thermal conductivity, thermophoresis, and Brownian motion parameters are raised?
5. Does an increase in the magnitude of solutal stratification, chemical reaction, Peclet number, and bioconvection Lewis number affect the mass transfer and microorganism density number of the Carreau fluid conveying tiny particles?

2 | RESEARCH METHODOLOGY

The flow coupled with heat and mass transfer of two-dimensional, incompressible, and steady electrically conducting Carreau fluid conveying tiny particles with thermomigration and haphazard movement of the tiny particles is developed over a stretchy surface in the presence of variable viscosity and thermal conductivity. As illustrated in Figure 1, the flow dynamics is set up with coordinate (x,y) having corresponding velocity components as (u,v) shown as the x-axis is taken along the vertically stretching sheet in the direction of flow with the y-axis normal to it. The sheet stretches with a velocity $u = U_w = ax$, where $a > 0$ is the stretching constant, a uniform external magnetic field B_0 is inclined to the flow direction while the induced magnetic field is ignored due to sufficiently low magnetic Reynolds number, stratification effects, nonlinear radiative heat flux together with exponential space-based heat source are incorporated. With these assumptions together with the Oberbeck–Boussinesq and boundary layer approximations, the formulated governing equations for magnetohydrodynamic

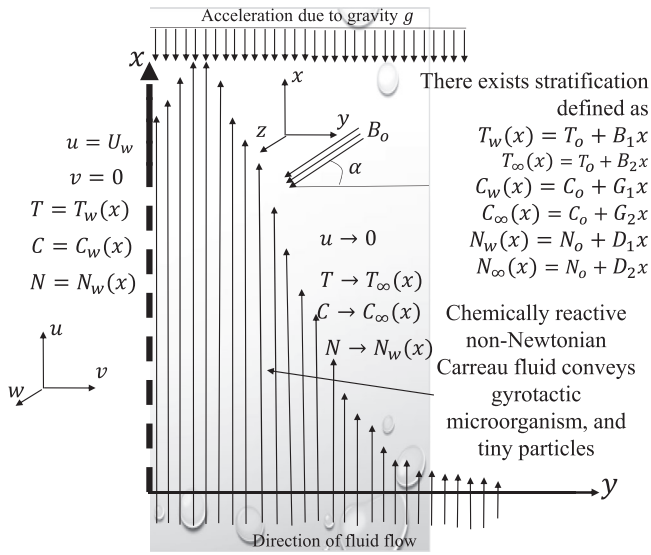

FIGURE 1 Physical configuration in the xy-domain

Carreau nanoliquid featuring continuity equation, momentum equation, energy transfer, concentration, and motile microorganism equations are communicated by Alsaedi et al.,[45] Al-Khaled et al.,[46] and Muntazir et al.[47] as

$$\frac{\partial u}{\partial x}+\frac{\partial v}{\partial y}=0, \tag{1}$$

$$\begin{aligned} u\frac{\partial u}{\partial x}+v\frac{\partial u}{\partial y}=&\frac{1}{\rho_{f\infty}}\frac{\partial}{\partial y}\left(\mu_f(T)\frac{\partial u}{\partial y}\right)+\frac{3}{2}(n-1)\Gamma^2\frac{1}{\rho_{f\infty}}\frac{\partial}{\partial y}\left(\mu_f(T)\frac{\partial u}{\partial y}\right)\left(\frac{\partial u}{\partial y}\right)^2-\frac{\sigma B_0^2}{\rho_{f\infty}}\sin^2\alpha u\\ &+\frac{1}{\rho_{f\infty}}[(1-\phi_f)\rho_{f\infty}\beta_1(T-T_\infty)g-(\rho_p-\rho_{f\infty})(\phi-\phi_\infty)g\\ &-\beta_2(N-N_\infty)(\rho_n-\rho_{f\infty})g], \end{aligned} \tag{2}$$

$$\begin{aligned} \frac{\partial T}{\partial x}+v\frac{\partial T}{\partial y}=&\frac{1}{(\rho_\infty c_p)_f}\frac{\partial}{\partial y}\left(k_f\frac{\partial T}{\partial y}\right)+\frac{\sigma B_0^2}{(\rho_\infty c_p)_f}\sin^2\alpha u^2+\frac{Q_0(T_w-T_0)}{(\rho_\infty c_p)_f}\exp\left(-my\sqrt{\frac{b}{\nu_\infty}}\right)\\ &+\frac{16\sigma^\star}{3k_\star(\rho c_p)_f}\frac{\partial}{\partial y}\left(T^3\frac{\partial T}{\partial y}\right)+\chi\left(\frac{\partial T}{\partial y}\right)\left[\frac{D_T}{T_\infty}\left(\frac{\partial T}{\partial y}\right)+D_B\left(\frac{\partial C}{\partial y}\right)\right], \end{aligned} \tag{3}$$

$$u\frac{\partial C}{\partial x}+v\frac{\partial C}{\partial y}=D_B\frac{\partial^2 C}{\partial y^2}+\frac{D_T}{T_\infty}\frac{\partial^2 T}{\partial y^2}-k_r(C-C_\infty), \tag{4}$$

$$u\frac{\partial N}{\partial x}+v\frac{\partial N}{\partial y}+\frac{\kappa W_c}{(C_w-C_\infty)}\frac{\partial}{\partial y}\left(N\frac{\partial C}{\partial y}\right)=D_N\frac{\partial^2 N}{\partial y^2}. \tag{5}$$

At an angle of α, the magnetic field has a nonzero inclination (angle between the direction of the vector B and another preferred direction); see Figure 1 and Equations (2) and (3). The conditions at the boundary are

$$\begin{aligned} &u=U_w=ax,\quad v=0,\quad T=T_w(x)=T_0+B_1x,\quad C=C_w(x)=C_0+G_1x,\\ &N=N_w(x)=N_0+D_1x\quad \text{at } y=0, \end{aligned} \tag{6}$$

where u and v indicate the velocity in the x and y directions, respectively, U_w denotes the stretching velocity whereas T_0, C_0, and N_0 are referred to as reference temperature, reference concentration of nanoparticles, and reference motile microorganism, respectively. As $y\to\infty$, the boundary conditions are

$$\begin{aligned} &u\to 0,\quad T\to[T_\infty=T_0+B_2x],\quad C\to[C_\infty=C_0+G_2x],\quad N\to[N_\infty=N_0+D_2x]\quad \text{as}\\ &y\to\infty. \end{aligned} \tag{7}$$

The temperature-dependent viscosity and thermal conductivity are sequentially written as (Theuri and Makinde,[48] Ali and Makinde,[49] Chiam,[50] Das et al.,[51] and Animasaun et al.[52])

$$\mu(T)=\mu_\infty e^{-q(T-T_\infty)},\quad k=k_\infty[1+h(T-T_\infty)], \tag{8}$$

where μ_∞ and k_∞ orderly indicates the free stream viscosity and free stream thermal conductivity. The fourth term on the right-hand side of the energy equation (3) indicates the nonlinear radiation term. In the transport of Carreau fluid with tiny particles, the radiative heat equation for optically thick media has accounted for the radiative heat flux in the energy equation. This term has been included on the assumption that the temperature difference within the layers of the Carreau fluid conveying tiny particles with motile microorganism is not sufficiently small. In this view, it becomes unrealistic to simplify the radiative heat flux as linear Taylor series expansion but with implicit differentiation, the partial rate of change of higher-order terms is evaluated as done by Koriko et al.[38] With the introduction of the quantities in Equation (9), the governing equations have been translated into ordinary differential equations.

$$\eta = y\sqrt{\frac{a}{\nu_\infty}},\quad \psi = \sqrt{a\nu_\infty}xf(\eta),\quad \theta(\eta) = \frac{T - T_\infty}{T_w - T_0},\quad \phi(\eta) = \frac{C - C_\infty}{C_w - C_0},$$
$$\xi(\eta) = \frac{N - N_\infty}{N_w - N_0},\quad Re_x = \frac{a^2x}{\nu_\infty}. \tag{9}$$

On substituting Equation (9) into the governing equations (1)–(5) together with the boundary conditions equations (6) and (7) taking cognizance of Equation (8), the continuity equation (1) becomes valid. Thus obtain

$$e^{-b\theta}\left(1 + \frac{3}{2}(n-1)(We)^2f''2\right)f''' - b\left(1 + \frac{3}{2}(n-1)(We)^2f''^2\right)e^{-b\theta}f''\theta' - M\sin^2\alpha f' + ff'' - f'^2 + \lambda(\theta - Nr\phi - R\xi) = 0, \tag{10}$$

$$\left[1 + \varepsilon\theta + Rd\left(1 + \left(\frac{\theta}{s + \theta_r}\right)\right)^3\right]\theta'' + \left(\frac{3Rd}{\theta_r + s}\right)\left(1 + \left(\frac{\theta}{s + \theta_r}\right)\right)^2\theta'^2 + \varepsilon\theta'^2 + PrQe^{-m\eta} + Pr(f\theta' - f'\theta - rsf' + MEc\sin^2\alpha f'^2 + NT\theta'^2 + Nb\theta'\phi') = 0, \tag{11}$$

$$\phi'' + Sc(f\phi' - f'\phi - Gf') + \frac{NT}{Nb}\theta'' - \gamma_r Sc\phi = 0, \tag{12}$$

$$\xi'' + Lb(f\xi' - f'\xi - Jf') - Pe(\xi'\phi' + (\xi + \Omega)\phi'') = 0. \tag{13}$$

The conditions at the boundary also become

$$f'(0) = 1,\ f(0) = 0,\ \theta(0) = 1 - s,\ \phi(0) = 1 - G,\ \xi(0) = 1 - J, \tag{14}$$

$$f'(\infty) = 0,\ \theta(\infty) = 0,\ \phi(\infty) = 0,\ \xi(\infty) = 0. \tag{15}$$

The emerging physical parameters are described below:

$$Pr = \frac{\nu_\infty (c_p)_f}{k_\infty}, \quad M = \frac{\sigma B_0^2}{a\rho_{f\infty}}, \quad LB = \frac{\nu_\infty}{D_B}, \quad Nb = \frac{\chi D_B (C_w - C_0)}{\nu_\infty}, \quad Lb = \frac{\nu_\infty}{D_N}, \quad s = \frac{B_2}{B_1},$$
$$J = \frac{D_2}{D_1}, \quad NT = \frac{\chi D_T (T_w - T_0)}{T_\infty \nu_\infty}, \quad \Omega = \frac{N_\infty}{N_w - N_\infty}, \quad Q = \frac{Q_0}{a(\rho c_p)_f}, \quad Ec = \frac{u_w^2}{c_{pf}(T_w - T_0)},$$
$$Pe = \frac{\kappa W_c}{D_N}, \quad \gamma_r = \frac{k_r}{a}, \quad Nr = \frac{(\rho_p - \rho_f)(C_w - C_0)}{(1 - \phi_\infty)\rho_f \beta_1 (T_w - T_0)}, \quad Rd = \frac{16\sigma^* T_\infty^3}{3k^* k_f}, \quad b = q(T_w - T_0),$$
$$\theta_r = \frac{T_w}{T_0}, \quad \lambda = \frac{(1 - \phi_\infty) g \beta_1 (T_w - T_0)}{a^2 x}, \quad We = \sqrt{\frac{\Gamma^2 a^3 x^2}{\nu_\infty}}, \quad \varepsilon = h(T_w - T_0), \quad G = \frac{G_2}{G_1},$$
$$R = \frac{(N_w - N_0)\beta_2 (\rho_n - \rho_{n\infty})}{(1 - \phi_\infty)\rho_{f\infty} \beta_1 (T_w - T_0)}, \quad Sc = \frac{\nu_\infty}{D_B}. \tag{16}$$

Various symbols in the governing equations are designated in Table 1.

2.1 | Quantities of engineering interest

The quantities of interest for the current study are the skin friction coefficient C_{fx}, local Nusselt number Nu_x, Sherwood number Sh_x, and the microorganism density number Sn_x are, respectively, defined as

$$C_{fx} = \frac{\tau_w}{\rho_\infty u_w^2}, \quad Nu_x = \frac{x q_w}{k_\infty (T_w - T_0)}, \quad Sh_x = \frac{x q_m}{D_B (C_w - C_0)}, \quad Sn_x = \frac{x q_h}{D_N (N_w - N_0)}, \tag{17}$$

$$\tau_w = \mu_f \left(\frac{\partial u}{\partial y} + \left(\frac{n-1}{2} \right) \Gamma^2 \left(\frac{\partial u}{\partial y} \right)^2 \right) \Bigg|_{y=0}, \quad q_w = -\left(k_\infty + \frac{16 T^3 \sigma^\star}{3k^\star} \right) \frac{\partial T}{\partial y} \Bigg|_{y=0}, \tag{18}$$

$$q_m = -D_B \frac{\partial C}{\partial y} \Bigg|_{y=0}, \quad q_h = -D_N \frac{\partial N}{\partial y} \Bigg|_{y=0}, \tag{19}$$

where τ_w indicates the surface shear stress, q_w denotes the surface heat flux, q_m is the surface mass flux, and q_n is the surface flux for the motile microorganisms. Substituting Equation (9) into Equation (17), the dimensionless C_{fx} is written in Equation (20) while that of Nu_x and Sh_x are, respectively, presented in Equations (21) and (22).

$$C_{fx} = Re_x^{-\frac{1}{2}} \left[f''(0) + \left(\frac{n-1}{2} \right) (We)^2 f''^2(0) \right], \tag{20}$$

$$Nu_x = -Re_x^{\frac{1}{2}} [1 + Rd(1 + (\theta_r - 1)\theta(0))^3] \theta'(0), \tag{21}$$

$$Sh_x = -Re_x^{\frac{1}{2}} \phi'(0), \quad Sn_x = -Re_x^{\frac{1}{2}} \xi'(0). \tag{22}$$

TABLE 1 Symbols and nomenclature

Symbols	Nomenclature	Symbols	Nomenclature
u, v	Velocity in the x, y direction	T	Temperature
ν_f	Kinematic viscosity	C	Concentration of nanoparticles
ρ_f	Fluid density	N	Concentration of microorganism
μ_f	Fluid viscosity	U_w	Velocity at the sheet
σ	Electrical conductivity	g	Gravitational acceleration
$(\rho c_p)_f$	Heat capacity of the fluid	n	Power-law index
k	Thermal conductivity	T_∞	Temperature at free stream
ρ_f	Nanofluid density	C_∞	Concentration at the free stream
ρ_p	Nanoparticle density	N_∞	Ambient concentration of microorganism
ρ_m	Microorganism density	$k^\star$	Mean absorption coefficient
$(\rho c_p)_f$	Heat capacity of nanoparticle	W_c	Maximum cell swimming speed
D_B	Brownian diffusion coefficient	D_T	Thermophoretic diffusion coefficient
D_N	Diffusivity of microorganism	β_1	Volumetric expansion coefficient
a	Stretching constant	β_2	Average volume of a microorganism
α	Inclination angle		
$\varkappa$	Chemotaxis constant	Q	Coefficient of volumetric heat source
b	Viscosity parameter	λ	Mixed convection parameter
Pr	Prandtl number	Ω	Microorganisms concentration difference
Rd	Radiation parameter	R	Bioconvection Rayleigh number
Ec	Eckert number	Nr	Buoyancy ratio parameter
Lb	Bioconvection Schmidt number	Sc	Schmidt number
s	Thermal stratification term	G	Solute stratification term
J	Microorganism stratification	We	Weissenberg number
Pe	Peclet number	ε	Thermal conductivity parameter
θ_r	Wall heating temperature ratio term	γ_r	Chemical reaction term
M	Magnetic field parameter	Q	Heat generation parameter
NT	Thermophoresis parameter	Nb	Brownian motion parameter

3 | NUMERICAL METHOD AND ITS VALIDATION

Due to the nonlinearity of the set of equations arrived at in this study, a numerical approach has been sought to provide the needed solution to the governing equations. In this study, the Runge–Kutta–Gill technique in MATLAB bvp4c is applied to obtain the solution to the system of Equations (10)–(14) subject to Equation (14).

4 | ANALYSIS OF RESULTS AND DISCUSSION

Various graphs have been sketched in this part to verify the substantial contributions of altering physical parameters concerning dimensionless quantities for a better understanding of their influence. There are also appropriate explanations of various parameter impacts. Figures 2 and 3 show the flow momentum response to an increasing viscosity term (b) value and the Weissenberg number (We) along the stream, respectively. A decrease in the velocity profile is caused by an increase in the quality of viscosity b, as seen in Figure 2. As the viscosity is increased, the internal friction of the gyrotactic motile microorganisms for the nanofluid is increased to oppose the Carreau nanoparticles' free flow. The bonding force is increased, causing the relative motion of the neighboring fluid layers to increase, and the flow velocity to decrease. As a result of the higher stresses, viscosity induces deformation of fluid components, resulting in velocity field damping. Figure 3 shows the flow viscoelastic characteristic as an increasing Weissenberg number (We). The movement of the Carreau nanofluid is shown to be accelerated as the magnitude of We increases. The flow dimension was dominated by the elastic forces of the motile bacteria compared to the viscous forces, resulting in a rising velocity profile. Because the mass reaction of the nanofluid is increasing and the heat conductivity of the fluid particles is increasing, the time rate of fluid stress relaxation is increasing. Figures 4 and 5 show the effect of increasing physical quantities, Brownian motion (Nb), and the chemical reaction term (γ_r) on the nanoparticle concentration field. The quantities Nb and γ_r, which represent Brownian motion and chemical reaction, respectively, slowed down the volume concentration of the magneto-Carreau fluid reaction, resulting in a narrower mass distribution. Figure 4 shows how a slight random movement of gyrotactic bacteria along the unbounded stream prevents liquid particle dispersion. As a result, as the Brownian motion was increased, the concentration profile decreased due to poor nanoparticle contact and

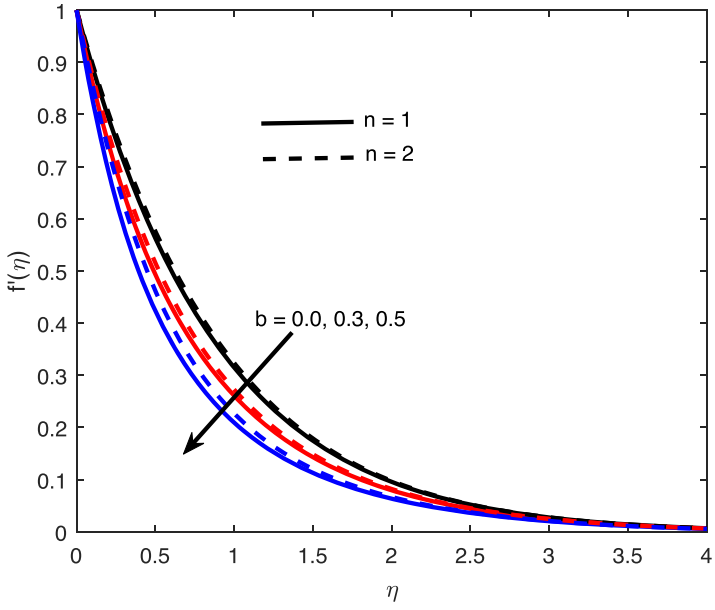

FIGURE 2 Velocity profiles at different levels of b

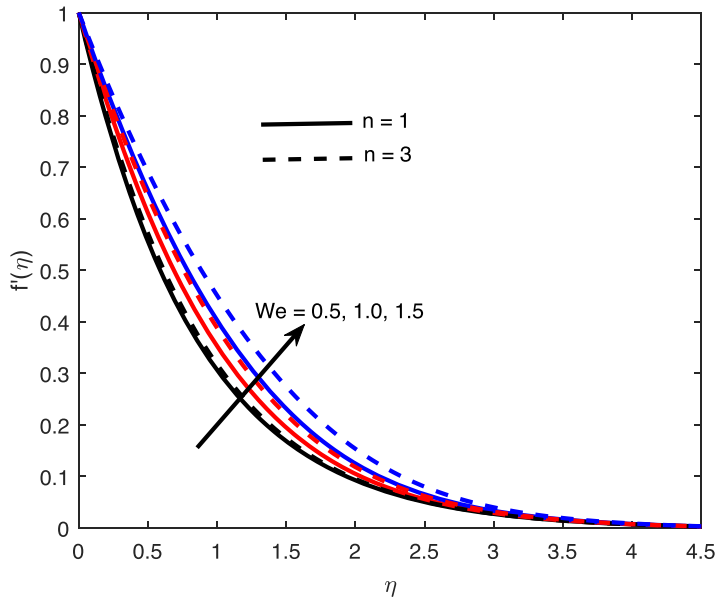

FIGURE 3 Velocity profiles at different levels of *We*

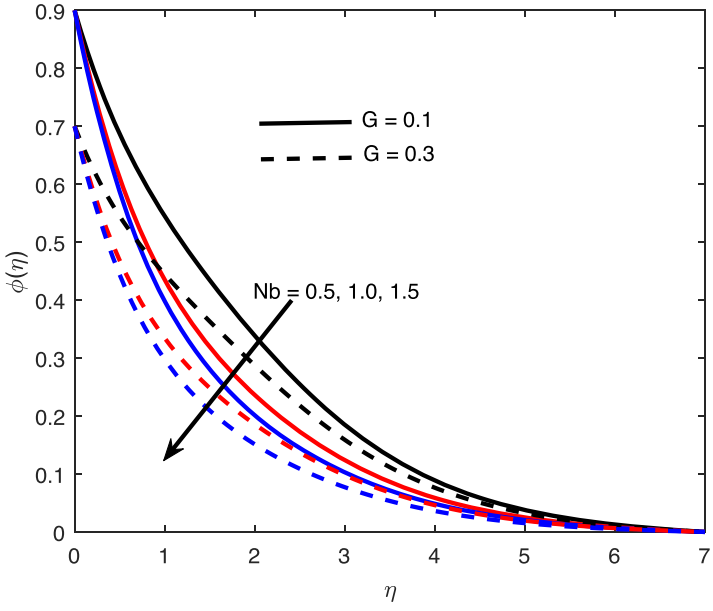

FIGURE 4 Concentration profiles at different levels of *Nb*

heat diffusion. In addition, the mass transfer profile of the Carreau nanofluid reactant mixes is discouraged in Figure 5 due to significant magneto-nanoparticle bonding. Due to the lack of activation energy and low heat output, fluid species mixtures formed, causing the concentration field to decrease as chemical reaction values increased.

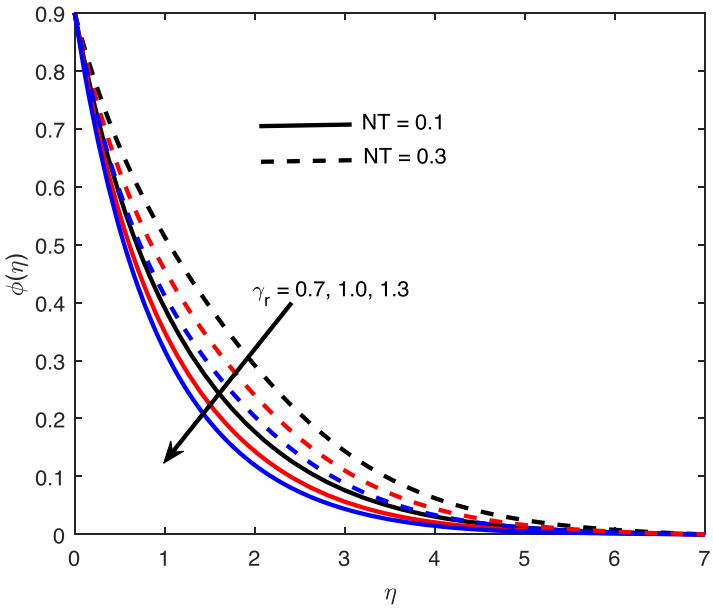

FIGURE 5 Concentration profiles at different levels of γ_1

Figures 6 and 7 show the effects of an exponential space-based volumetric heat source Q and a wall heating/temperature ratio θ_r on the heat distribution, with the Eckert number ($Ec = 0.1, 0.7$) varied. In the presence of gyrotactic motile microorganisms, the temperature field increased as a result of multiple response mechanisms of magneto-Carreau nanofluid. The conductivity of the nanofluid is increased, resulting in increased heat propagation and a rising temperature profile. The improved thermal boundary layer structure, which reduces ambient heat transport, also supports this. As a result, as the volumetric heat source increased, the heat dispersion increased. Meanwhile, in Figure 7, the temperature of the investigated absolute viscoplastic fluid characteristic was dominated by the absolute stretching surface temperature ratio under varying thermal conductivity. As the temperature ratio is increased, the temperature profile falls through the stream regime. In the meantime, when Ec rises, the temperature distribution advances, as seen in both images. The increased heat created by friction between the Carreau nanofluid particles owing to viscous dissipation caused this development. The thermal conductivity of the non-Newtonian Carreau fluid conveying microscopic particles improves as the dissipation grows, resulting in a larger thermal boundary layer structure. Figures 8 and 9 demonstrate the physical terms viscosity (b) and Weissenberg number (Wb) for different power-law exponents on temperature distribution. As seen in Figure 8, as heat is created internally to break the Carreau nanoparticle bonding force, a rising viscosity implies increased heat diffusivity. As a result, the liquid particles interact forcefully to overcome the fluid viscosity's pulling effect and boost nanoparticle heat dispersion, which stimulates a heat transfer profile. In contrast, Figure 9 depicts the temperature field reaction to increasing Weissenberg number, indicating a decreasing impact on heat transmission. To increase the viscoplastic property of the nanofluid Carreau flow reaction mixtures, the viscous forces guided the elastic forces of the fluid mixtures. As a result, the stress relaxation rate and a

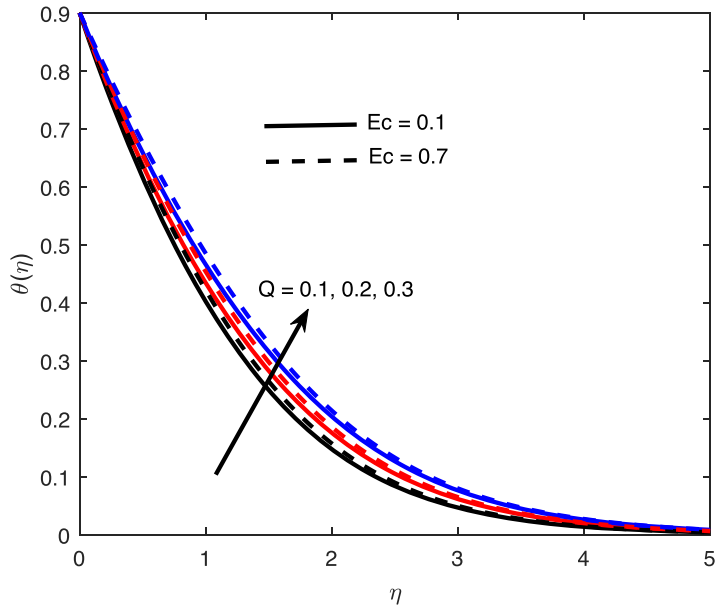

FIGURE 6 Temperature profiles at different levels of Q

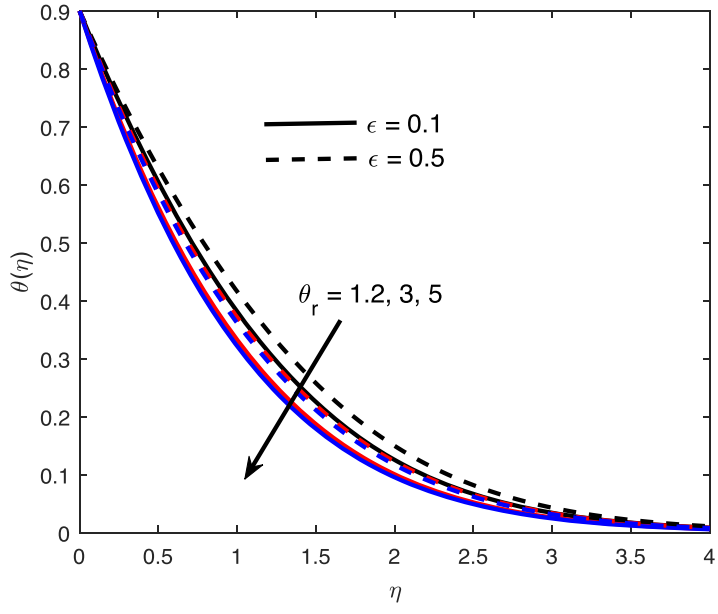

FIGURE 7 Temperature profiles at different levels of θ_r

heat source are discouraged, resulting in a decrease in the response rate and temperature propagation profile.

The impact of thermophoresis (NT) and radiation (Rd) on the heat distribution of the magneto-Carreau nanofluid reaction for different thermal stratification (s) values is shown in Figures 10 and 11. Because of the high stimulation of the boundary layer viscosity, which

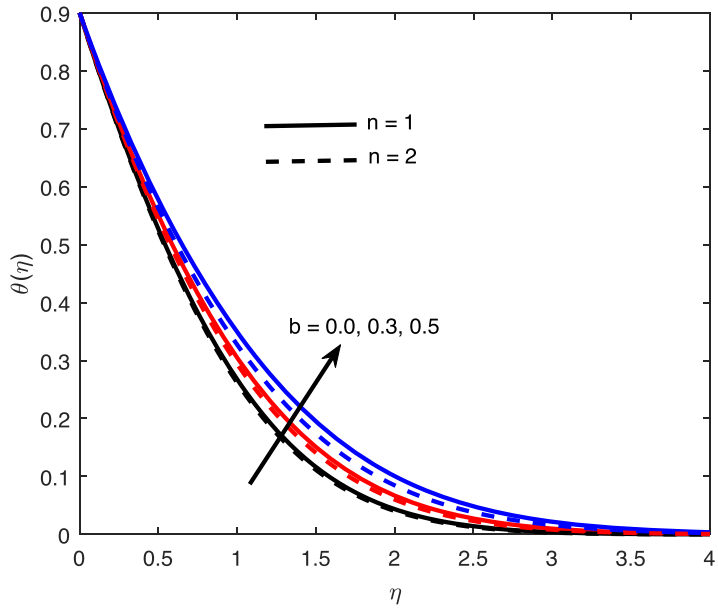

FIGURE 8 Temperature profiles at different levels of b

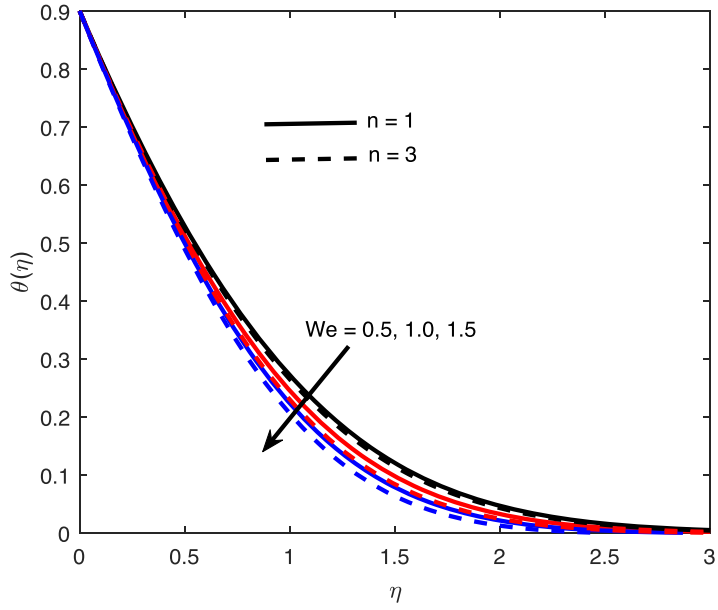

FIGURE 9 Temperature profiles at different levels of We

inhibits ambient heat transfer, the temperature profiles improved with an increase in both dimensionless parameters. Thermophoresis is the reaction of a mobile particle to a temperature gradient, whereas radiation is the transfer of energy through a material medium. As a result, the terms (NT) and (Rd) propel the fluid particles' gyrotactic motion, causing growing heat

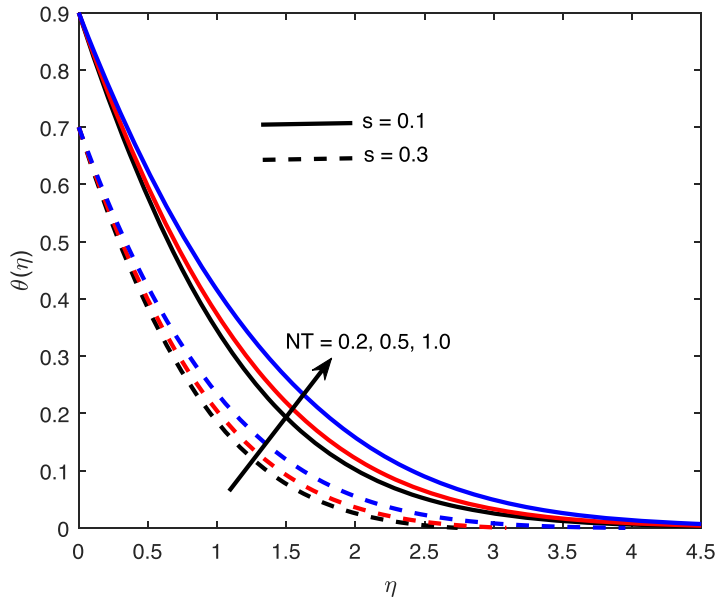

FIGURE 10 Temperature profiles at different levels of *NT*

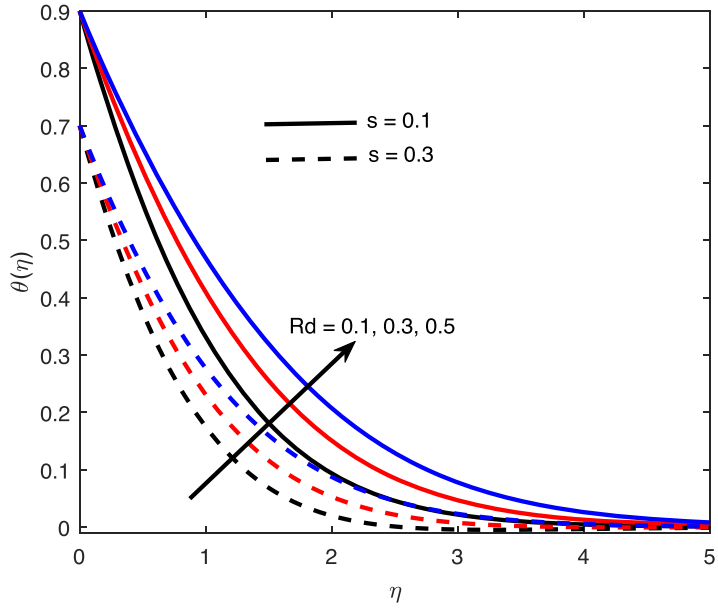

FIGURE 11 Temperature profiles at different levels of *Rd*

distribution throughout the limitless stretchable device. The heated particles are dragged away from the hotter to the cooler zone when (NT) grows, raising the gyrotactic Carreau nanofluid temperature, as shown in Figure 10. Similarly, increases in the magnitude of (s) lead the Carreau nanofluid density in the lower area to increase in contrast to the upper. As a result, the

temperature differential between the heated surface and the upstream field decreased, resulting in a decrease in fluid temperature. This observation is consistent with those of Atif et al.[40] and Hayat et al.[53] As shown in Figures 12 and 13, an increase in the microorganism concentration difference (Ω) and motile microorganism stratification term (J), along with variations in the bioconvective Schmidt number (Lb) and Peclet number (Pe), reduces the microorganism concentration mass profile. These variables increased the chemical bonding of gyrotactic motile microorganisms and decreased the contact of nanoparticles, which slow down chemical reaction mixtures. As a result, the occurrence dampens the distribution of microbe concentrations at varied boundary conditions. A rise in Lb has a decreasing influence on the Carreau fluid microbe density profile, as can be seen in Figure 12. The ratio of the motile microorganism's momentum diffusivity is defined by this parameter. As a result, increasing Lb values raise the momentum diffusivity rate, which then dominates the microorganism diffusion rate, resulting in a decrease in motile microbe density profile. As clearly depicted, a rise in J lowers the motile density profile. This trend occurs owing to a reduction in the concentration difference of the gyrotactic microorganism between the surface and upstream region. Also, an enhancement in the values of the Peclet number (Pe) depreciates the motile density profile as found in Figure 13. This is because, as Pe escalates in magnitudes, the motile microorganism diffusivity declines, also there is an improvement in the movement of fluid particles leading to a decreased thickness of motile microorganisms as such, the motile density distribution is reduced. These reactions conform with the results of Ferdows et al.[54] and that of Abbas et al.[55]

Table 2 demonstrates the effect of a few selected factors on the skin friction coefficient C_{fx}. The skin friction coefficient C_{fx} is found to be enhanced by increasing the magnitude of the viscosity variation term b, angle of inclination α, and magnetic field parameter M, whereas the skin friction coefficient C_{fx} is reduced by increasing the magnitude of the Weissenberg number We and mixed convection parameter λ. The friction between the fluid and the stretched material rises as the fluid

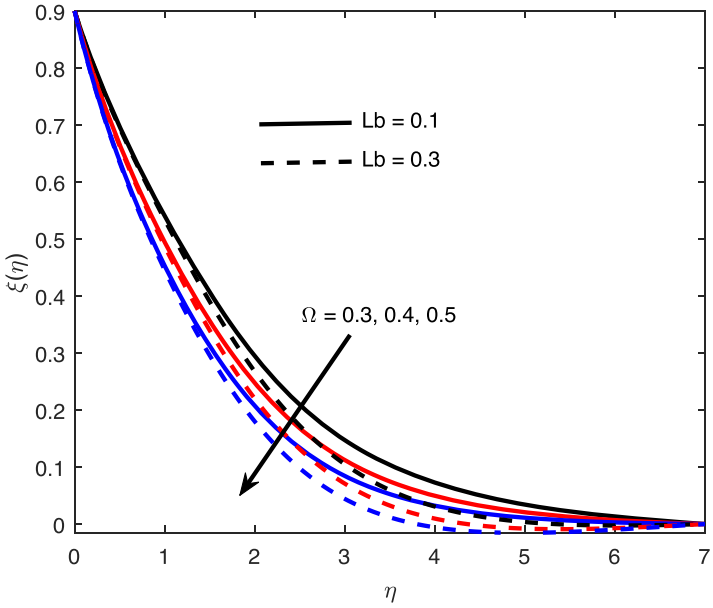

FIGURE 12 Microorganism profiles at different levels of Ω

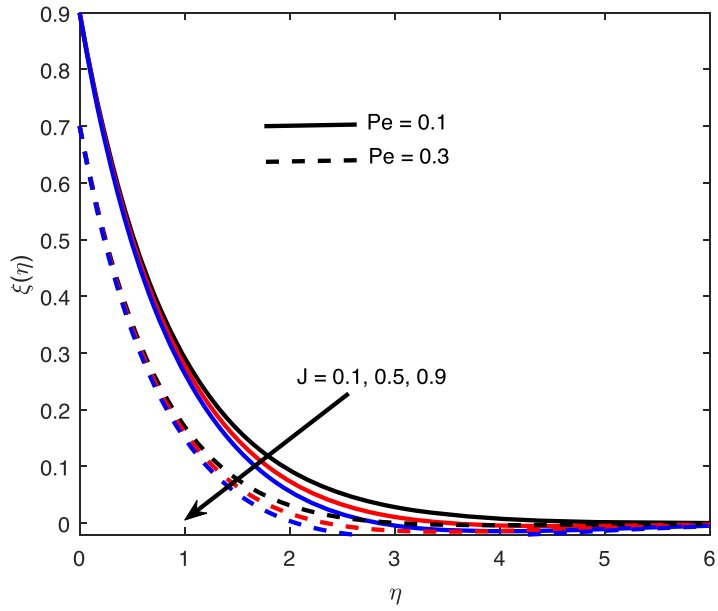

FIGURE 13 Microorganism profiles at different levels of J

TABLE 2 Computational values of C_{fx} for variations in b, We, α, λ, and M

b	We	α	λ	M	C_{fx}
0.0	0.3	60°	0.1	0.5	1.11827
0.3					1.29734
0.5					1.42032
0.2	0.5				1.19021
	1.0				1.06313
	1.5				0.95854
	0.3	30°			1.12283
		60°			1.23664
		90°			1.28909
		60°	0.1		1.23664
			0.3		1.16955
			0.5		1.10426
			0.1	0.1	1.09839
				0.5	1.23664
				0.7	1.29927

TABLE 3 Computational values of Nu_x and Sh_x for variations in s, θ_r, ε, NT, and Nb

s	θ_r	ε	NT	Nb	Nu_x
0.1		0.2	0.5	0.3	0.70917
0.3					0.73616
0.5					0.74736
0.1	1.2				0.66414
	3.0				0.80015
	5.0				0.83446
	1.5	0.1			0.72932
		0.3			0.69042
		0.5			0.65652
		0.2	0.2		0.75172
			0.5		0.70917
			1.0		0.64856
			0.5	0.5	0.66668
				1.0	0.57212
				1.5	0.49351

TABLE 4 Computational values of Sh_x and Sn_x for variations in G, γ_r, and Lb and Pe

G	γ_r	Lb	Pe	Sh_x	Sn_x
0.1	0.3	1.2	1.2	0.13007	1.12571
0.3				0.01548	1.02148
0.5				0.09939	0.91941
0.1	0.7			0.39003	1.39283
	1.0			0.53581	1.54809
	1.3			0.65861	1.68162
	0.3	0.1		0.12841	0.30933
		0.3		0.12905	0.50048
		0.5		0.12947	0.66812
			0.1	0.12982	1.03122
			0.3	0.12987	1.04797
			0.5	0.12992	1.06492

gets more viscous, and the draglike force (Lorentz force) created as a result of the transverse magnetic field boosts the skin friction coefficient as M grows. However, when We increases, the Carreu nanofluid viscosity decreases, and friction decreases. Similarly, when λ increases, the buoyancy force takes precedence over the viscous force, resulting in a reduction in viscous drag. Table 3 shows the

effects of the thermal stratification term s, the wall heating/temperature ratio term θ_r, the thermal conductivity parameter ε, thermophoresis NT, and Brownian motion Nb parameters on the Nusselt Nu_x. The Nusselt number, which relates to heat transport at the surface, increases as the thermal stratification parameter increases for $0.1 \leq s \leq 0.5$. As seen in this table, increasing the size of the temperature ratio parameter θ_r enhances heat transmission. However, as shown in Table 3, an increase in the thermal conductivity term ε, the thermophoresis parameter NT, and Brownian motion Nb reduce heat transport over the stretched surface. For changes in solute stratification term G, chemical reaction parameter γ_r, bioconvection Lewis number Lb, and Peclet number Pe, the computational values of the Sherwood number Sh_x and motile microbe density number Sn_x are shown in Table 4. This table shows that increasing γ_r, Lb, and Pe improves both Sh_x and Sn_x, but mass transfer, as well as motile microbe density number, decreases with solute stratification term G.

5 | CONCLUSION

In the report, the outcome of the study on the heat transfer across the dynamics of Carreau fluid subject to inclined Lorentz force conveying tiny particles and motile gyrotactic microorganisms with emphasis on three kinds of stratification (i.e., thermal, concentration, and diffusion of motile microorganisms). On the basis of the analysis and discussion of results, it is worth concluding that:

- The velocity $f'(\eta)$ against the monotonically increasing stream length η shows a declining or rising profile for respective variation in the terms viscosity parameter b and Weissenberg number We.
- The heat propagation along the boundless flow stream is boosted for rising terms value Q, b, NT, and Rd but decreased for increasing values We and θ_r. The heat transfer across the surface improves with the enhancement of s and θ_r whereas a decline in the heat transfer occurs with the terms ε, NT, and Nb.
- Carreau nanofluid concentration boundary layer structure and chemical mixtures diminished for increased values of the term Nb and γ_r.
- The gyrotactic motile microorganism profile is a decreasing function of the terms Lb, Ω, J, and Pe.

As a consequence, the study will help develop biotechnology and industrial productivity in fields, including hydromagnetic lubricants, ecological engineering, microsystems, and others. In the future, additional research into stretchable concentric cylinder flow with Arrhenius kinetics response may be conducted.

DATA AVAILABILITY STATEMENT

The data that support the findings of this study are available on request from the corresponding author. The data are not publicly available due to privacy or ethical restrictions.

ORCID

I. L. Animasaun http://orcid.org/0000-0002-5553-2587
A. S. Oke http://orcid.org/0000-0003-3903-4112
S. O. Salawu http://orcid.org/0000-0001-6951-7524

REFERENCES

1. Animasaun IL, Shah NA, Wakif A, Mahanthesh B, Sivaraj R, Koriko OK. *Ratio of Momentum Diffusivity to Thermal Diffusivity: Introduction, Meta-analysis, and Scrutinization*. Chapman and Hall/CRC; 2022. ISBN-13: 978-1032108520, ISBN-10: 1032108525, ISBN9781003217374.
2. Shamshuddin M, Mabood F, Salawu SO. Flow of three-dimensional radiative Williamson fluid over an inclined stretching sheet with Hall current and nth-order chemical reaction. *Heat Transfer*. 2021;50(6): 5400-5417. doi:10.1002/htj.22130
3. Ahmad R, Farooqi A, Farooqi R. An analytical approach to study the blood flow over a nonlinear tapering stenosed artery in flow of Carreau fluid model. *Complexity*. 2021;2021:1-11.
4. Jangili S, Adesanya SO, Ogunseye HA, Lebelo R. Couple stress fluid flow with variable properties: a second law analysis. *Math Methods Appl Sci*. 2018;42(1):85-98. doi:10.1002/mma.5325
5. Hassan AR, Salawu SO, Disu AB. The variable viscosity effects on hydromagnetic couple stress heat generating porous fluid flow with convective wall cooling. *Sci Afr*. 2020;9:e00495. doi:10.1016/j.sciaf.2020.e00495
6. Barakat EII. Variable viscosity effect on hydromagnetic flow and heat transfer about a fluid underlying the axisymmetric spreading surface. *Acta Mech*. 2004;169(1-4):195-202. doi:10.1007/s00707-004-0075-4
7. Mahmoud MA. Variable fluid properties effects on hydromagnetic fluid flow over an exponentially stretching sheet. *Open Sci J Math Appl*. 2015;3(2):26-33.
8. Salawu SO, Oderinu RA, Ohaegbue AD. Thermal runaway and thermodynamic second law of a reactive couple stress hydromagnetic fluid with variable properties and Navier slips. *Sci Afr*. 2020;7:e00261. doi:10.1016/j.sciaf.2019.e00261
9. Pratumwal Y, Limtrakarn W, Muengtaweepongsa S, et al. Whole blood viscosity modeling using power law, Casson, and Carreau Yasuda models integrated with image scanning U-tube viscometer technique. *Songklanakarin J Sci Technol*. 2017;39(5):625-631.
10. Abdollahzadeh Jamalabadi MY, Daqiqshirazi M, Nasiri H, Safaei MR, Nguyen TK. Modeling and analysis of biomagnetic blood Carreau fluid flow through a stenosis artery with magnetic heat transfer: a transient study. *PLoS ONE*. 2018;13(2):e0192138. doi:10.1371/journal.pone.0192138
11. Vadasz P, ed. *Emerging Topics in Heat and Mass Transfer in Porous Media: From Bioengineering and Microelectronics to Nanotechnology*. Vol 22. Springer Science & Business Media, Springer; 2008:133-147.
12. Tsai T-H, Liou D-S, Kuo L-S, Chen P-H. Rapid mixing between ferro-nanofluid and water in a semi-active Y-type micromixer. *Sens Actuators A: Phys*. 2009;153(2):267-273. doi:10.1016/j.sna.2009.05.004
13. Yusuf TA, Akaje TW, Salawu SO, Gbadeyan JA. Arrhenius activation energy effect on a stagnation point slippery MHD Casson nanofluid flow with entropy generation and melting heat transfer. *Defect and Diffus Forum*. 2021;408:1-18. doi:10.4028/www.scientific.net/ddf.408.1
14. Nima NI, Salawu SO, Ferdows M, Shamshuddin M, Alsenafi A, Nakayama A. Melting effect on non-Newtonian fluid flow in gyrotactic microorganism saturated non-Darcy porous media with variable fluid properties. *Appl Nanosci*. 2020;10(10):3911-3924. doi:10.1007/s13204-020-01491-y
15. Kuznetsov AV, Avramenko AA. Effect of small particles on this stability of bioconvection in a suspension of gyrotactic microorganisms in a layer of finite depth. *Int Commun Heat Mass Transfer*. 2004;31(1):1-10. doi:10.1016/s0735-1933(03)00196-9
16. Beg OA, Uddin MJ, Khan WA. Bioconvective non-Newtonian nanofluid transport in porous media containing micro-organisms in a moving free stream. *J Mech Med Biol*. 2015;15(05):1550071. doi:10.1142/s0219519415500712
17. Mahdy A. Natural convection boundary layer flow due to gyrotactic microorganisms about a vertical cone in porous media saturated by a nanofluid. *J Braz Soc Mech Sci Eng*. 2015;38(1):67-76. doi:10.1007/s40430-015-0313-9
18. Han S, Zhang Q, Zhang X, et al. A digital microfluidic diluter-based microalgal motion biosensor for marine pollution monitoring. *Biosens Bioelectron*. 2019;143:111597. doi:10.1016/j.bios.2019.111597
19. Song Y-Q, Waqas H, Al-Khaled K, et al. Bioconvection analysis for Sutterby nanofluid over an axially stretched cylinder with melting heat transfer and variable thermal features: a Marangoni and solutal model. *Alexandria Eng J*. 2021;60(5):4663-4675. doi:10.1016/j.aej.2021.03.056

20. Choi SUS. *Enhancing Thermal Conductivity of Fluids with Nanoparticle*. Vol 66. ASME; 1995: 99-105. FED 231/MD.
21. Qayyum S, Khan MI, Hayat T, Alsaedi A. Comparative investigation of five nanoparticles in flow of viscous fluid with Joule heating and slip due to rotating disk. *Phys B: Condens Matter*. 2018;534:173-183. doi:10.1016/j.physb.2018.01.044
22. Salawu SO, Fatunmbi EO, Okoya SS. MHD heat and mass transport of Maxwell Arrhenius kinetic nanofluid flow over stretching surface with nonlinear variable properties. *Results Chem*. 2021;3:100125. doi:10.1016/j.rechem.2021.100125
23. Fatunmbi EO, Salawu SO. Analysis of hydromagnetic micropolar nanofluid flow past a nonlinear stretchable sheet and entropy generation with Navier slips. *Int J Modelling Simul*. 2021;42(3):359-369. doi:10.1080/02286203.2021.1905490
24. Khan MI, Qayyum S, Kadry S, Khan WA, Abbas SZ. Irreversibility analysis and heat transport in squeezing nanoliquid flow of non-Newtonian (second-grade) fluid between infinite plates with activation energy. *Arab J Sci Eng*. 2020;45(6):4939-4947. doi:10.1007/s13369-020-04442-5
25. Hayat T, Khan SA, Khan MI, Alsaedi A. Optimizing the theoretical analysis of entropy generation in the flow of second grade nanofluid. *Phys Scr*. 2019;94(8):085001. doi:10.1088/1402-4896/ab0f65
26. IjazKhan M, Alzahrani F. Numerical simulation for the mixed convective flow of non-Newtonian fluid with activation energy and entropy generation. *Math Methods Appl Sci*. 2020;44(9):7766-7777. doi:10.1002/mma.6919
27. Niu J, Fu C, Tan W. Slip-flow and heat transfer of a non-Newtonian nanofluid in a microtube. *PLoS ONE*. 2012;7(5):e37274. doi:10.1371/journal.pone.0037274
28. Fatunmbi EO, Adeosun AT. Nonlinear radiative Eyring–Powell nanofluid flow along a vertical Riga plate with exponential varying viscosity and chemical reaction. *Int Commun Heat Mass Transfer*. 2020;119:104913. doi:10.1016/j.icheatmasstransfer.2020.104913
29. Oke AS, Animasaun IL, Mutuku WN, Kimathi M, Shah NA, Saleem S. Significance of Coriolis force, volume fraction, and heat source/sink on the dynamics of water conveying 47 nm alumina nanoparticles over a uniform surface. *Chin J Phys*. 2021;71:716-727. doi:10.1016/j.cjph.2021.02.005
30. Kinyanjui Kigio J, Winifred Nduku M, Abayomi Samuel O. Analysis of volume fraction and convective heat transfer on MHD Casson nanofluid over a vertical plate. *Fluid Mech*. 2021;7(1):1. doi:10.11648/j.fm.20210701.11
31. Fatunmbi EO, Mabood F, Elmonser H, Tlili I. Magnetohydrodynamic nonlinear mixed convection flow of reactive tangent hyperbolic nano fluid passing a nonlinear stretchable surface. *Phys Scr*. 2020;96(1):015204. doi:10.1088/1402-4896/abc3e9
32. Song Y-Q, Obideyi BD, Shah NA, Animasaun IL, Mahrous YM, Chung JD. Significance of haphazard motion and thermal migration of alumina and copper nanoparticles across the dynamics of water and ethylene glycol on a convectively heated surface. *Case Stud Therm Eng*. 2021;26:101050. doi:10.1016/j.csite.2021.101050
33. Mabood F, Fatunmbi EO, Benos L, Sarris IE. Entropy generation in the magnetohydrodynamic Jeffrey nanofluid flow over a stretching sheet with wide range of engineering application parameters. *Int J Appl Comput Math*. 2022;8(98):1-18. doi:10.1007/s40819-022-01301-9
34. Khan NS, Islam S, Gul T, Khan I, Khan W, Ali L. Thin film flow of a second grade fluid in a porous medium past a stretching sheet with heat transfer. *Alexandria Eng J*. 2018;57(2):1019-1031. doi:10.1016/j.aej.2017.01.036
35. Khan NS, Gul T, Islam S, Khan W. Thermophoresis and thermal radiation with heat and mass transfer in a magnetohydrodynamic thin-film second-grade fluid of variable properties past a stretching sheet. Eur Phys J Plus. 2017;132(11). doi:10.1140/epjp/i2017-11277-3
36. Khan N, Gul T, Islam S, Khan I, Alqahtani A, Alshomrani A. Magnetohydrodynamic nanoliquid thin film sprayed on a stretching cylinder with heat transfer. *Appl Sci*. 2017;7(3):271. doi:10.3390/app7030271
37. Khan NS, Gul T, Khan MA, Bonyah E, Islam S. Mixed convection in gravity-driven thin film non-Newtonian nanofluids flow with gyrotactic microorganisms. *Results Phys*. 2017;7:4033-4049. doi:10.1016/j.rinp.2017.10.017
38. Koriko OK, Animasaun IL, Omowaye AJ, Oreyeni T. The combined influence of nonlinear thermal radiation and thermal stratification on the dynamics of micropolar fluid along a vertical surface. *Multidiscip Model Mater Struct*. 2019;15(1):133-155. doi:10.1108/mmms-12-2017-0155

39. Rehman KU, Malik MY, Salahuddin T, Naseer M. Dual stratified mixed convection flow of Eyring–Powell fluid over an inclined stretching cylinder with heat generation/absorption effect. *AIP Adv*. 2016;6(7):075112. doi:10.1063/1.4959587
40. Atif SM, Hussain S, Sagheer M. Magnetohydrodynamic stratified bioconvective flow of micropolar nanofluid due to gyrotactic microorganisms. *AIP Adv*. 2019;9(2):025208. doi:10.1063/1.5085742
41. Ijaz M, Ayub M. Activation energy and dual stratification effects for Walter-B fluid flow in view of Cattaneo–Christov double diffusion. *Heliyon*. 2019;5(6):e01815. doi:10.1016/j.heliyon.2019.e01815
42. Sarojamma G, Vijaya Lakshmi R, Sreelakshmi K, Vajravelu K. Dual stratification effects on double-diffusive convective heat and mass transfer of a sheet-driven micropolar fluid flow. *J King Saud Univ—Sci*. 2020;32(1):366-376. doi:10.1016/j.jksus.2018.05.027
43. Abbas T, Rehman S, Shah RA, Idrees M, Qayyum M. Analysis of MHD Carreau fluid flow over a stretching permeable sheet with variable viscosity and thermal conductivity. *Phys A: Stat Mech Appl*. 2020;551:124225. doi:10.1016/j.physa.2020.124225
44. Shah RA, Abbas T, Idrees M, Ullah M. MHD Carreau fluid slip flow over a porous stretching sheet with viscous dissipation and variable thermal conductivity. Boundary Value Problems. 2017;94(2017). doi:10.1186/s13661-017-0827-4
45. Alsaedi A, Khan MI, Farooq M, Gull N, Hayat T. Magnetohydrodynamic (MHD) stratified bioconvective flow of nanofluid due to gyrotactic microorganisms. *Adv Powder Technol*. 2017;28(1):288-298. doi:10.1016/j.apt.2016.10.002
46. Al-Khaled K, Khan SU, Khan I. Chemically reactive bioconvection flow of tangent hyperbolic nanoliquid with gyrotactic microorganisms and nonlinear thermal radiation. *Heliyon*. 2020;6(1):e03117. doi:10.1016/j.heliyon.2019.e03117
47. Muntazir RMA, Mushtaq M, Jabeen K. A numerical study of MHD Carreau nanofluid flow with gyrotactic microorganisms over a plate, wedge, and stagnation point. *Math Problems Eng*. 2021;2021(1):1-22. doi:10.1155/2021/5520780
48. Theuri D, Makinde OD. Thermodynamic analysis of variable viscosity MHD unsteady generalized Couette flow with permeable walls. Appl Comput Math. 2014;3(1):1-8 doi:10.11648/j.acm.20140301.11
49. Ali A, Makinde OD. Modelling the effect of variable viscosity on unsteady Couette flow of nanofluids with convective cooling. *J Appl Fluid Mech*. 2015;8(4):793-802. doi:10.18869/acadpub.jafm.67.223.22967
50. Chiam TC. Heat transfer in a fluid with variable thermal conductivity over a linearly stretching sheet. *Acta Mech*. 1998;129(1-2):63-72. doi:10.1007/bf01379650
51. Das K, Jana S, Kundu PK. Thermophoretic MHD slip flow over a permeable surface with variable fluid properties. *Alexandria Eng J*. 2015;54(1):35-44. doi:10.1016/j.aej.2014.11.005
52. Animasaun IL, Adebile EA, Fagbade AI. Casson fluid flow with variable thermophysical property along exponentially stretching sheet with suction and exponentially decaying internal heat generation using the homotopy analysis method. *J Niger Math Soc*. 2016;35(1):1-17. doi:10.1016/j.jnnms.2015.02.001
53. Hayat T, Qayyum S, Alsaedi A, Ahmad B. Mechanisms of double stratification and magnetic field in flow of third grade fluid over a slendering stretching surface with variable thermal conductivity. *Results Phys*. 2018;8:819-828. doi:10.1016/j.rinp.2017.12.057
54. Ferdows M, Reddy MG, Sun S, Alzahrani F. Two-dimensional gyrotactic microorganisms flow of hydromagnetic power law nanofluid past an elongated sheet. *Adv Mech Eng*. 2019;11(11):1687814019881252. doi:10.1177/1687814019881252
55. Abbas T, Hayat T, Ayub M, Bhatti MM, Alsaedi A. Electromagnetohydrodynamic nanofluid flow past a porous Riga plate containing gyrotactic microorganism. *Neural Comput Appl*. 2019;31(6):1905-1913.

How to cite this article: Fatunmbi EO, Animasaun IL, Oke AS, Salawu SO. Insight into the heat transfer across the dynamics of Carreau fluid subject to inclined Lorentz force conveying tiny particles and motile gyrotactic microorganisms: The case of stratification. *Heat Transfer*. 2022;51:7562-7583. doi:10.1002/htj.22655